Theor Chem Account (2008) 120:85–94
DOI 10.1007/s00214-007-0302-x

REGULAR ARTICLE

Tetra-hydrides of the third-row transition elements: spin–orbit coupling effects on geometrical deformation in WH_4 and OsH_4

Taka-aki Hisashima · Takeshi Matsushita · Toshio Asada · Shiro Koseki · Azumao Toyota

Received: 20 November 2006 / Accepted: 12 February 2007 / Published online: 8 May 2007

Abstract The dissociation energies of MH_4 (M = La, Hf–Hg) were computed using full optimized reaction space (FORS) multi-configuration self-consistent field (MCSCF) and second-order multi-reference Møller–Plesset perturbation methods with the SBKJC basis sets augmented by a set of polarization functions (SBKJC(f,p)). It was shown that of the molecules examined, only four tetra-hydrides HfH_4, TaH_4, WH_4, and OsH_4 with T_d symmetry are lower in energy than the corresponding dissociation limits. For WH_4 and OsH_4, the potential energy surfaces from the D_{4h} to the T_d structure were explored from both theoretical calculations and symmetry arguments based on the pseudo-Jahn- Teller effect. As for WH_4, it is found that the ground state could be ^3E_g, $^3A_{2g}$, or $^3B_{2g}$ at the D_{4h} structure. The present calculations suggest that the ground state is ^3E_g, and that this state is stabilized by the e_u deformation into a C_{2v} structure ($^3B_1$) and then sequentially to the most stable T_d structure ($^3A_2$). If the molecular system is promoted to the lowest $^3B_{2g}$ state, the D_{4h} structure can directly deform into the most stable T_d structure along the b_{2u} vibrational mode. For OsH_4, the ground state ($^5B_{1g}$) at the D_{4h} structure deforms into a D_{2d} structure and the resulting $^5B_2$ state strongly interacts with the lowest ^3E and $^1A_1$ states due to the spin-orbit couplings (SOCs). As a result, it was shown that the relativistic potential energy of the lowest spin-mixed state (ground state) monotonically decreases along the D_{2d} deformation path from the D_{4h} to the T_d structure.

Keywords Pseudo-Jahn-Teller deformation · Tetra-hydrides of third-row transition elements · Spin–orbit coupling

1 Introduction

Recently, much attentions have been paid to relativistic effects in molecules [1–7]. These effects frequently play important roles in studying chemical reactions, especially of heavy metal compounds. Although several research groups tried to solve the two-component or even four-component Dirac equations of molecules and reported interesting results [8–16], relativistic effective core potential (RECP) and model core potential (MCP) methods have been employed in most theoretical studies [17–28]. In the RECP and MCP studies, the spin-independent parts (mass-velocity and Darwin terms) of the relativistic effects are included in the core potentials and the spin-dependent parts (spin–orbit and spin–spin couplings) are additionally included after orbital optimization. The spin–orbit couplings (SOCs) are rather interesting since they explain the electronic transitions between states of different spin multiplicity; this is the so-called "intersystem crossing." Our research group reported the basic results of transition metal hydrides using the effective nuclear charge (Z_{eff}) approximation for the Breit-Pauli Hamiltonian [29–37] and discussed the reliability of this approximation. We also applied this method to explain the emission processes of organic electro-luminescence (EL) and the design of more effective EL compounds [38,39].

Contribution to the Mark S. Gordon 65th Birthday Festschrift Issue.

Electronic supplementary material The online version of this article (doi:10.1007/s00214-007-0302-x) contains supplementary material, which is available to authorized users.

T. Hisashima · T. Matsushita · T. Asada · S. Koseki (✉)
Department of Chemistry, Graduate School of Science, Osaka Prefecture University, 1-1 Gakuen-cho, Naka-ku, Sakai, Osaka 599-8531, Japan
e-mail: shiro@c.s.osakafu-u.ac.jp

A. Toyota
Department of Chemistry, Faculty of Education, Arts and Science, Yamagata University, Yamagata 990-8560, Japan

We have also investigated the geometrical deformation paths of conjugated hydrocarbons on the basis of the pseudo-Jahn-Teller (or second-order Jahn-Teller) theory over the last two decades [40–51]. Our recent investigations have been concerned with the non-planarity of conjugated molecules [49–51], and the origin of force driving molecular systems to their final geometries has been clarified in order to apply them to the analysis and/or design of geometrical structures for large-sized conjugated hydrocarbons and carbon nanotubes.

Our recent interests are focused on the geometrical structures of transition metal complexes. As described above, the SOC effects play significantly important roles in determining the reaction mechanisms of such heavy metal compounds, especially those of the third-row transition elements. It is interesting to examine why the compounds containing heavy elements have complicated structures. During the first step of these investigations, the geometrical structures of simple hydrides should be investigated and, if some kinds of rules or trends can be obtained, they will be applied to the studies of larger molecular complexes. We have reported the spin-orbit splittings of low-lying electronic states in the first-, second-, and third-row transition elements [32,33] and the relativistic dissociation potential energy curves of low-lying electronic states in their mono-hydrides [34–37]. In these studies, an averaged error of 20 – 30% is found for the spin–orbit splittings obtained using the Z_{eff} approximation in the SOC calculations.

It is noted that the tungsten and osmium compounds are well-known catalyses for hydrogenation of certain compounds [52–55]. Also, the tungsten and osmium hydrides are used for hydrogen adsorption reactions, exchange reactions of hydrogen-deuterium, and hydrogen abstractions in alkenes [56–58]. Theoretically, the geometrical structures of WH_4 and OsH_4 have been studied by Bayse et al. [59] by means of the MP2 method with Christiansen's RECP basis sets [21,22]. They concluded that the most stable structures of WH_4 and OsH_4 are of D_{2d} and T_d symmetry, respectively. Experimentally, on the other hand, Wang et al. observed the IR spectrum of tungsten hydrides in low-temperature matrices and reported that WH_4 has the ground state $^3A_1$ at the T_d structure with the help of a DFT vibrational analysis [60].

Under these circumstances, we study here the ground-state electronic structures of tetra-hydrides of third-row transition elements. As will be shown below, since the four tetra-hydrides HfH_4, TaH_4, WH_4, and OsH_4 are lower in energy than their corresponding dissociation limits, we examine the stable geometrical structures of WH_4 and OsH_4 using the multi-configuration self-consistent field (MCSCF) method and employing the Z_{eff} approximation for the Breit-Pauli Hamiltonian to estimate the SOCs. It is remarked that to the best of our knowledge, no relativistic studies have yet been performed on these hydrides. On the basis of the pseudo Jahn-Teller effect, it will be shown that the structural changes for WH_4 and OsH_4 are explained within the adiabatic and relativistic pictures, respectively.

2 Methods of calculation

The optimization of the stationary structures for MH_4 (M = La, Hf–Hg), as well as MH_2, was performed using the full optimized reaction space (FORS) MCSCF method [61,62] with the SBKJC basis sets for the transition elements [17–20] and the 31G(p) basis set for the hydrogen atom. The MCSCF active space includes ten orbitals correlating to the 5*d* and 6*s* orbitals of a transition element and 1*s* orbitals of hydrogen atoms in the dissociation limit of MH_4. The dissociation limit was assumed to be placed at the distance of 30 Å between the transition element and the mass centers of hydrogen molecules. Since it is difficult to estimate basis-set superposition error (BSSE) using MCSCF methods, the BSSE was not considered and the binding energies could be overestimated in such investigations. This method is referred to as MCSCF/SBKJC in the following discussion.

The relative energies of these structures were re-estimated at the FORS MCSCF and MRMP2 levels of theory using the SBKJC basis sets augmented by a set of polarization functions, where a larger active space has been used (including 5*d*, 6*sp*, and hydrogen's 1*s* orbitals in the dissociation limit) and MRMP2 is the abbreviations for the multi-reference second-order Møller–Plesset perturbation theory [63]. These methods are referred to as MCSCF/SBKJC(f,p) and MRMP2/SBKJC(f,p).

In order to construct the SOC matrices, the MCSCF/SBKJC optimized orbitals were employed, in which these matrix elements were computed using the Z_{eff} approximation [29–31]. In order to keep the size of the matrices computationally tractable, SOC matrices include the adiabatic states whose energies are lower in energy than a specific upper limit of energies: the upper limit was set to −69.120 (WH_4) or −92.530 (OsH_4) hartree along the entire deformation paths of the molecular structures. All these calculations were carried out using the GAMESS suite of program codes [64].

3 Results and discussion

3.1 Highest symmetrical structures of MH_4

The trivial high symmetry for MH_4 must be T_d and D_{4h}. The T_d and D_{4h} geometrical structures of MH_4 are optimized for states of various multiplicities and symmetries using the MCSCF/SBKJC method. Table 1 lists the ground-state symmetries and the internuclear distances of the M–H bonds. Since the T_d and D_{4h} symmetries were maintained during

Table 1 M–H distances (Å) and state symmetries of the ground states at the high symmetric structures of MH_4 obtained using the MCSCF/SBKJC method

MH_4	T_d		D_{4h}		$MH_2 + H_2$		H − M − H
LaH_4	2.274	$^2T_2$	2.241	^2E_u	2.158	$^2A_1$	111.6
					2.104[a]		
HfH_4	1.871	$^1A_1$	1.916	$^1A_{1g}$	1.858	$^1A_1$	123.8
					1.865[a]		
TaH_4	1.804	^2E	1.862	$^2A_{1g}$	1.824	$^4A_2$	119.5
WH_4	1.746	$^3A_2$	1.821	^3E_g	1.766	$^5B_2$	117.6
					1.717[a]		
ReH_4	1.684	^2E	1.802	^6E_u	1.812	$^6\Sigma_g^+$	180.0
					1.745[a]		
OsH_4	1.630	$^1A_1$	1.748	$^5B_{2g}$	1.636	$^3B_1$	106.5
IrH_4	1.622	$^2T_2$	1.716	$^2A_{2u}$	1.584	$^2A_1$	90.1
PtH_4	1.640	$^3T_2$	1.683	^3E_u	1.549	$^1A_1$	84.8
					1.521[a]		
AuH_4	1.735	$^4A_1$	1.673	^2E_u	1.647	$^2B_2$	126.7
					1.619[a]		
HgH_4	1.904	^1E	1.672	$^1A_{1g}$	1.692	$^1\Sigma_g^+$	180.0
					1.642[a]		

For MH_2, M–H distances (Å), ground-state symmetries, and H–M–H angle (deg.) are listed. Previously reported data: La–H = 2.08 Å(MCSCF+SOCI) [71]. Hf–H = 1.907 for HfH_4 [65]. Ta–H = 1.763–1.776 Å(MP2/ECP) [73]. W–H = 1.720 Å(B3LYP) for WH_2 and W–H = 1.712 Å(B3LYP) for WH_4 [60]. W–H = 1.84–1.99 Å(DFT) [74]. Re–H = 1.753 Å(B3LYP) for ReH_2 and Re–H = 1.649 Å(B3LYP) for ReH_4 [67]. Os–H = 1.615–1.693 Å(B3LYP) or 1.580–1.616 Å(MP2) [72]. Ir–H = 1.570 Å($^4\sum^-$, B3LYP) for IrH^+ [70]. Au–H = 1.619 Å(B3LYP) for AuH_2 and Au–H = 1.649 Å(B3LYP) for AuH_4^- [68]. Au–H = 1.59–1.62 Å(CASSCF) [69]

[a] See [65] M–H bond lengths were obtained using the BPW91 method

geometry optimizations, specific structures were obtained as shown in Table 1. These results indicate that the T_d and D_{4h} structures are explicitly lower in energy than M + 4H (or their atomization energies are positive). The present investigation employs $MH_2 + H_2$ and $M + 2H_2$ as the dissociation limits. The bond length (0.753 Å) of the hydrogen molecules and the geometrical structures of di-hydrides (MH_2) in the dissociation limit were also optimized for their ground states at the MCSCF/SBKJC level of theory (see Table 1). The geometrical structures and their ground-state symmetries for MH_2 are mostly in agreement with those reported by Andrews [65][1].

Table 2 lists the relative energies of the T_d and D_{4h} structures to the corresponding dissociation limits ($MH_2 + H_2$) obtained using the MCSCF/SBKJC(f,p) and MRMP2/SBKJC(f,p) methods. The table shows that HfH_4, TaH_4, WH_4, and OsH_4 could be formed as stable tetra-hydrides with T_d structures. The normal mode analyses proved that their Hessians are positive definite. It also suggests that the other T_d and all D_{4h} structures are explicitly higher in energy than the corresponding dissociation limits, $MH_2 + H_2$ and/or $M + 2H_2$. Therefore, these would easily dissociate into $MH_2 + H_2$ or $M + 2H_2$ along C_{2v} or lower symmetrical paths, and it should be difficult to experimentally detect these tetra-hydrides. To the best of our knowledge, few experimental reports have been found for tetra-hydrides of the third-row transition elements, even though several experimental and theoretical reports can be found for di-hydrides and their ions [66–74].

These results can be explained as follows: the M–H bonds in a T_d structure are constructed by the hybridization of the M's 6*s*, $5d_{xy}$, $5d_{xz}$, and $5d_{yz}$ orbitals and by four hydrogen 1*s* orbitals. These bonds correspond to the highest and next highest occupied molecular orbitals, t_2 (HOMO) and a_1 (next HOMO). For HfH_4, the main electron configuration of the ground state has a closed-shell structure,

$$^1A_1 : (\text{core})(\text{Hf5s})^2(\text{Hf5p})^6(a_1)^2(t_2)^6.$$

This is consistent with the result of Bayse et al. [63] and experimental results [75], where Bayse et al. discussed the geometrical structures of MH_n (n = 3–9) using the "Orbitally Ranked Symmetry Analysis Method" (ORSAM).

[1] The present calculations provide that HfH_2 and ReH_2 have a singlet ground state at a bent structure and a sextet ground state at a linear structure, respectively (see Table 1). However, Andrews concluded that the HfH_2 ground state is triplet ($^3B_1$) and a bent structure ($^6A_1$) is more stable in ReH_2.

Table 2 Relative energies (kcal/mol) of the high symmetric structures of MH_4 obtained using the MCSCF/SBKJC(f,p) and MCSCF+MRMP2/SBKJC(f,p) methods

	T_d		D_{4h}		MH_2+H_2		$M+2H_2$	M[a]
LaH_4	(51.4)	$^2T_2$	63.0	^2E_u	0.0	$^2A_1$	17.9	^2D
	(51.5)		60.8		0.0		12.3	
HfH_4	−40.0	$^1A_1$	16.3	$^1A_{1g}$	0.0	$^1A_1$	27.8	^3F
	−38.0		14.5		0.0		24.1	
TaH_4	−39.2	^2E	2.8	$^2A_{1g}$	0.0	$^4A_2$	2.2	^4F
	−37.4		11.1		0.0		8.0	
WH_4	−19.3	$^3A_2$	53.3	^3E_g	0.0	^5B	20.7	^5D[b]
	−24.6		54.5		0.0		23.3	
ReH_4	29.7	^2E	55.0	^6E_u	0.0	$^6\sum_g^+$	−5.4	^6S
	11.4		44.8		0.0		−2.7	
OsH_4	−29.5	$^1A_1$	9.2	$^5B_{2g}$	0.0	$^3B_1$	−2.0	^5D
	−42.8		15.9		0.0		5.4	
IrH_4	13.0	$^2T_2$	77.6	$^2A_{2u}$	0.0	$^2A_1$	11.0	^4F
	−0.1		77.1		0.0		32.2	
PtH_4	64.8	$^3T_2$	70.2	^3E_u	0.0	$^1A_1$	36.6	^3D[c]
	61.3		74.4		0.0		54.1	
AuH_4	78.5	$^4A_1$	42.3	^2E_u	0.0	$^1B_2$	−18.5	^2S
	70.1		34.6		0.0		−9.3	
HgH_4	136.5	^1E	58.1	$^1A_{1g}$	0.0	$^1\sum_g^+$	−30.3	^1S
	132.7		48.0		0.0		−26.1	

1st row = MCSCF, 2nd row = MCSCF+MRMP2. D(La–H)=60.0 kcal/mol (MCSCF) [71]. D(W–H)=3.6–9.8 kcal/mol (BP86) [74]. The values in *parentheses* are obtained using the MCSCF and MRMP2/SBKJC methods. The state degeneracy was broken, when the SBKJC(f,p) basis sets and the larger MCSCF active space were employed

[a] Ground state in atom (M)

[b] The ^7S state in W atom is calculated to be lower in energy than ^5D by 6.3 (MCSCF) or 8.2 (MRMP2) kcal/mol, but the $^5D_2$ spin-mixed state is the ground state in relativistic calculations [36]

[c] The ground state in Pt atom is calculated to be ^3F at the MCSCF/SBKJC(f,p) level of theory, but the MRMP2 calculation makes ^3D the ground state

Accordingly, LaH_4 should have an open site in the t_2 orbitals, and, as a result, this molecule ($^2T_2$) must be unstable. This is the reason why LaH_3, instead of LaH_4, has been investigated [76]. HfH_4 has vacant 5d $_{z^2}$ and 5d $_{x^2-y^2}$ orbitals, and these orbitals are classified into non-bonding molecular orbitals (NBMOs) and belong to the "e" irreducible representation in the T_d symmetry. These orbitals are the lowest unoccupied molecular orbitals (LUMOs). This explains the stabilization of TaH_4, WH_4, ReH_4, and OsH_4. The main electron configurations in their ground states are:

$$TaH_2,\ ^2E : (\text{core})(Ta5s)^2(Ta5p)^6(a_1)^2(t_2)^6(e)^1$$
$$WH_4,\ ^3A_2 : (\text{core})(W5s)^2(W5p)^6(a_1)^2(t_2)^6(e)^2$$
$$ReH_2,\ ^2E : (\text{core})(Re\,5s)^2(Re\,5p)^6(a_1)^2(t_2)^6(e)^3$$
$$OsH_4,\ ^1A_1 : (\text{core})(Os5s)^2(Os5p)^6(a_1)^2(t_2)^6(e)^4$$

The 5d $_{z^2}$ and 5d $_{x^2-y^2}$ orbitals, or NBMOs of MH_4, are fully occupied in OsH_4. As shown in Table 2, both WH_4 and OsH_4 have the most stable T_d structures, but Bayse et al. [59] concluded that WH_4 has a D_{2d} structure. Since the DFT calculations and the IR spectroscopy reported by Wang et al. [60] suggested that WH_4 has a T_d structure, we would conclude here that WH_4 is not a Jahn-Teller molecule and has the most stable T_d structure.

The T_d structure of ReH_4 is calculated to be higher in energy than the dissociation limit $ReH_2 + H_2$ using the present methods of calculation. Even though the Hessian cannot be computed for this degenerate state ^2E using GAMESS, it is found that this molecule is a Jahn-Teller molecule and slightly deforms into a D_{2d} structure. The degenerate ground state splits into $^2A_1$ and $^2B_1$ and the latter becomes the ground state at the D_{2d} optimized structure. The energy difference between the $^2E(D_{4h})$ and $^2B_1(D_{2d})$ states is calculated to be rather small at the MCSCF/SBKJC, MCSCF/SBKJC(f,p), and MRMP2/SBKJC(f,p) levels of theory. Additionally, the stabilization energy is also estimated

to be less than one kcal/mol at these three levels, and the D_{2d} structure is still higher in energy than the dissociation limit $ReH_2 + H_2$. Since Wang and Andrews reported that ReH_4 has a binding energy of about 26 kcal/mol [77], more sophisticated calculations might need to be performed.

On the basis of the above discussion, additional electrons in IrH_4, PtH_4, AuH_4, and HgH_4 must occupy the anti-bonding orbitals of M–H bonds and make these molecules unstable. These results suggest that IrH_3, PtH_2, and AuH may be stable. In fact, IrH_3, PtH_2 and AuH have been investigated by several research groups [78–86], even though the other kinds of hydrides may exist such as AuH_2 [65,68,69].

All the D_{4h} structures are higher in energy than the dissociation limit MH_2+H_2 as shown in Table 2. OsH_4 has relatively small energy difference between its D_{4h} structure and the corresponding dissociation limit $OsH_2 + H_2$. The main electron configuration of the ground state $^5B_{1g}$ at the D_{4h} structure is

$$(\text{core})(\text{Os5s})^2(\text{Os5p})^6(a_{1g})^2(b_{1g})^2(e_u)^4(e_g)^2(a_{1g})^1(b_{2g})^1.$$

The a_{1g} and e_u orbitals have large coefficients of H's 1*s* orbitals, and the Os's 6s and 5d $_{z^2}$ orbitals slightly contribute to the a_{1g} orbitals. The b_{1g} orbital is the bonding M–H orbital consisting of Os's 5d $_{x^2-y^2}$ and H's 1s orbitals. The e_g orbital is principally a set of Os's $5d_{xz}$ and $5d_{yz}$ orbitals, and the singly occupied a_{1g} and b_{2g} orbitals are Os's 5d $_{z^2}$ and $5d_{xy}$, respectively, where all these orbitals are NBMOs. Thus, the M–H bonding is mainly contributed by H's 1*s* orbitals and only by the Os's 6 *s* and 5d $_{x^2-y^2}$. This seems to be the main reason why such planar tetra-hydrides are unstable.

In the following sections, we discuss the calculated results for the geometrical deformation of WH_4 and OsH_4. The geometrical structures of HfH_4, TaH_4, and ReH_4 are being currently investigated in our laboratory, and the results will be reported in our forthcoming papers.

3.2 WH_4

As described in the previous section, the planar D_{4h} structure is much less stable than the corresponding T_d structure and is even less stable than the dissociation limit $WH_2 + H_2$ (see Table 3). The present section discusses the deformation path from the D_{4h} to the T_d structure on the basis of the pseudo-Jahn-Teller theory.

The ground state at the most stable T_d structure is $^3A_2$ and its Hessian matrix is positive definite as mentioned in the previous section. The main configuration of the ground state is

$$(\text{core})(\text{W5s})^2(\text{W5p})^6(a_1)^2(t_2)^6(e)^2.$$

From this configuration, electronic states $^1A_1$ and ^1E also arise. These singlet states are higher in energy than the $^3A_2$ state even after considering the effects of dynamic electron correlation. Wang et al. [60] reported that the ground state is $^3A_1$ at four DFT levels of theory. Unfortunately, the present methods predict that the lowest $^3A_1$ state is explicitly higher in energy than the $^3A_2$ state.

Table 3 Relative energies (kcal/mol) of the stationary structures in WH_4 and OsH_4 obtained using the MCSCF/SBKJC(f,p) and MRMP2/SBKJC(f,p) methods

			MCSCF[a]	MCSCF+MRMP2
WH_4	D_{4h}	^3E_g	0	0
		$^3A_{2g}$	+1.8 (3)	+4.3
		$^3B_{2g}$	+8.7 (3)	+10.8
	D_{2d}	^3E	−28.8	−36.5
	C_{2v}	$^3B_1$	−40.0 (1)	−43.2
	C_{4v}	$^3B_2$	−53.6 (1)	−61.1
	$C_s(1)$	$^3A'$	−56.2 (1)	−61.0
	T_d	$^3A_2$	−71.0 (0)	−79.1
$WH_2 + H_2$	C_{2v}	$^5B_2$	−53.3 (0)	−54.5
$W + 2H_2$		^5D	−32.5	−31.2
OsH_4	D_{4h}	$^5B_{1g}$	0 (3)	0
		$^1A_{1u}$	+67.7	+60.9
	D_{2d}	$^5B_2$	−7.7 (1)	−17.6
	C_{4v}	$^5B_1$	−8.2 (1)	−20.1
	C_s (1)	$^5A'$	−10.7 (0)	−21.4
	C_{2v}	$^5B_2$	−8.0 (1)	−17.3
	$C_s(2)$	$^5A''$	−12.6 (0)	−21.6
	T_d	$^1A_1$	−38.7 (0)	−58.8
$OsH_2 + H_2$	C_{2v}	$^3B_1$	−9.2 (0)	−15.9
$Os + 2H_2$		^5D	−11.2	−10.5

[a] The number in the parenthesis indicates the number of imaginary-frequency modes obtained using the MCSCF/SBKJC method

It is rather difficult to determine which state is the true ground state at the D_{4h} structure, since this structure is very high in energy and several low-lying electronic states are close in energy to each other. As shown in Table 3, the MCSCF/SBKJC(f,p) calculations indicate that the ground state is ^3E_g, but the energetic order of the low-lying states could be changed easily by the effects of dynamic electron correlation. The main configuration of the ^3E_g state is

$$(\text{core})(\text{W5s})^2(\text{W5p})^6(a_{1g})^2(b_{1g})^2(e_u)^4(e_g)^1(a_{1g})^1.$$

The singly occupied a_{1g} orbital principally consists of W's 5d z^2 and the lowest vacant b_{2g} orbital is the W's $5d_{xy}$ orbital. The main configuration of the lowest $^3A_{2g}$ state is

$$(\text{core})(\text{W5s})^2(\text{W5p})^6(a_{1g})^2(b_{1g})^2(e_u)^4(e_g)^2.$$

This state is only 1.8 kcal/mol higher than the ground state at the MCSCF level of theory, and the effects of dynamic correlation make the energy difference become slightly larger

(4.3 kcal/mol; see Table 3). Based on this electron configuration, three more singlet states ($^1A_{1g}$, $^1B_{1g}$, and $^1B_{2g}$) also arise. The $^3A_{2g}$ state is the lowest among these states, which obeys Hund's rule even after including the effects of dynamic electron correlation at the MCSCF + MRMP2 level of theory. The third state $^3B_{2g}$ is higher in energy than the ^3E_g state only by 8.7 (MCSCF) or 10.8 (MRMP2) kcal/mol.

Unfortunately, GAMESS cannot generate a Hessian matrix for the degenerate state ^3E_g. If this is a Jahn-Teller molecule, the geometry deformation takes place only in the molecular plane ($e_g \otimes e_g = a_{1g} + a_{2g} + b_{1g} + b_{2g}$) and never directly deforms into a non-planar T_d structure. The Hessian for the $^3A_{2g}$ state provides three imaginary-frequency modes (377i (a_{2u}), 924i (b_{2u}), and 488i (e_u)cm^{-1}), where the principal axis (z axis) is perpendicular to the molecular plane and the C_2' axes are on the linear H–W–H; the displacements along these vibrational modes derive the C_{4v}, D_{2d}, and C_{2v} structures, respectively (Fig. 1). Note that the Hessian for the $^3B_{2g}$ state also provides three imaginary-frequency modes (836i (a_{2u}), 1068i (b_{2u}), and 487i (e_u)cm^{-1}).

If the second lowest state $^3A_{2g}$ strongly interacts with $^3B_{1u}$ states, then the pseudo-Jahn-Teller theory predicts that the deformation along the b_{2u} mode occurs and that the $^3A_{2g}$ state correlates to the $^3A_2$ state at the D_{2d} structure. The present results show that only a shallow minimum exists on the lowest $^3A_2$ potential curve along this vibrational mode. The third state $^3B_{2g}$($^3B_1$ in D_{2d}) is rapidly stabilized along the b_{2u} mode by the interaction with $^3A_{1u}$ states and directly reaches the ground state $^3A_2$ at the most stable T_d structure after geometry optimization within D_{2d} symmetry. The ground state ^3E_g(^3E in D_{2d}) is also moderately stabilized along this vibrational mode by the interaction with ^3E_u states, but the optimized geometry still has a D_{2d} symmetry and is 42.2 (MCSCF) or 42.6 (MRMP2) kcal/mol higher in energy than the ground state $^3A_2$ at the most stable T_d structure (see Table 3). Thus, only when the molecular system is promoted to the $^3B_{2g}$ state at the D_{4h} structure, the deformation along the b_{2u} vibrational mode makes the molecular system be stabilized into the most stable T_d structure (see Scheme 1).

As mentioned above, both the $^3A_{2g}$ and $3B_{2g}$ states at the D_{4h} structure have two more imaginary-frequency modes (a_{2u} and e_u). The displacement along the a_{2u} mode energetically stabilizes the molecular system into a C_{4v} (square pyramid) structure (see Fig. 2). This is also explained by the pseudo-Jahn Teller theory as illustrated in Scheme 1; this deformations in the ^3E_g state is caused by the interaction with E_u states ($a_{2u} \in E_g \otimes E_u$), while those in the $^3A_{2g}$ and $^3B_{2g}$ states are caused by the interaction with $^3A_{1u}$ states ($a_{2u} \in A_{1u} \otimes A_{2g}$) and $^3B_{1u}$ states ($a_{2u} \in B_{1u} \otimes B_{2g}$), respectively. Along such deformation path, the ^3E_g,$^3A_{2g}$, and $^3B_{2g}$ states at the D_{4h} structure correlate to the ^3E,$^3A_2$, and $^3B_2$ states at the C_{4v} structure, respectively (see Scheme 1). The ground state is $^3B_2$ at the C_{4v} structure, and it is lower than the ground state ^3E_g at the D_{4h} structure by 53.6 (MCSCF) or 61.1 (MRMP2) kcal/mol. This ground state is calculated to have one imaginary-frequency mode. Accordingly, this structure sequentially deforms into the C_s structure (the $^3A'$ ground state; denoted by C_s (1) in Fig. 2). Furthermore, the C_s structure has one imaginary-frequency mode and deforms into the most stable T_d structure via a non-symmetrical path.

The last path is the deformation along the e_u mode (488i cm^{-1}) from the D_{4h} structure. This deformation provides two identical C_{2v} planar structures in which the molecular plane is taken as the yz plane. When the ^3E_g state at the D_{4h} structure suffers the e_u deformation, this state is split into A_2 and B_1 at the C_{2v} structure, while the $^3A_{2g}$ and $^3B_{2g}$ states in D_{4h} correlate to the $^3B_2$ and $^3A_1$ states at the C_{2v} structure, respectively. The ground state at the C_{2v} structure is not $^3B_2$ nor $^3A_1$, but $^3B_1$. Again, the ground state $^3B_1$ at the C_{2v} structure also has one imaginary-frequency mode (493i cm^{-1}) and its geometry deforms into a C_s structure and consequently into the most stable T_d structure via a non-symmetric path. Thus, it is found that the ground state ^3E_g at the D_{4h} structure can be stabilized into the most stable T_d structure along the e_u mode (see Scheme 1).

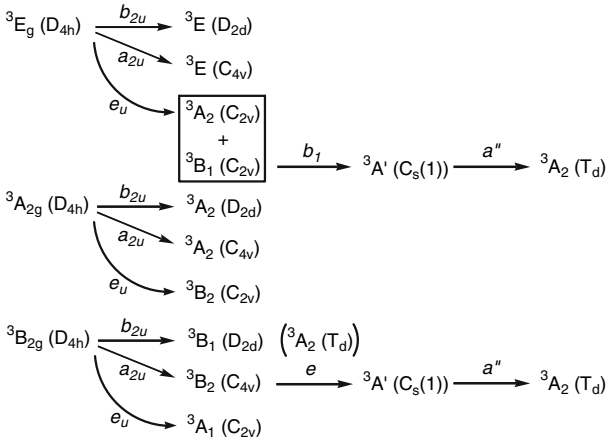

Scheme 1 Geometrical deformation paths from the D_{4h} structure to the T_d structure in WH_4

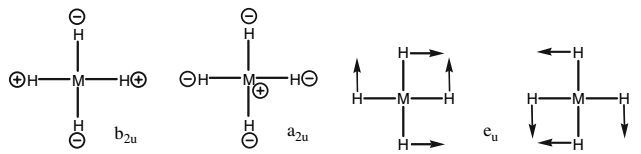

Fig. 1 Vibrational modes at the D_{4h} structure, where symmetry operations C_2' and σ_v are taken on linear H–M–H bonds

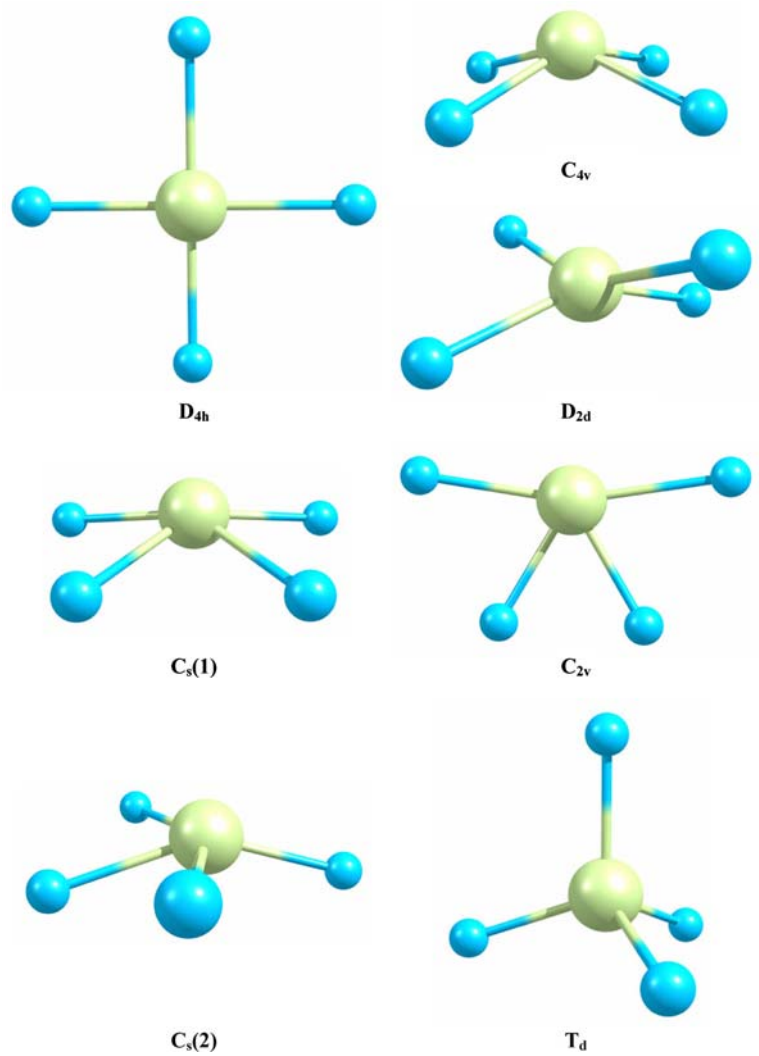

Fig. 2 Stationary structures illustrated by **ChemCraft** and their notations

3.3 OsH_4

The energy difference between the D_{4h} and T_d structures is much smaller than that for WH_4 (see Table 3). The energy difference between the D_{4h} structure and the dissociation limit $OsH_2 + H_2$ is also much smaller than that for WH_4, and the binding energy of the T_d structure is rather high.

At the most stable T_d structure of OsH_4, the ground state $^1A_1$ has a closed-shell configuration,

$$(\text{core})(\text{Os5s})^2(\text{Os5p})^6(a_1)^2(t_2)^6(e)^4.$$

Its Hessian matrix is positive definite. The dissociation energy to $OsH_2 + H_2$ is calculated to be 29.5 (MCSCF) or 42.8 (MRMP2) kcal/mol. Note that this dissociation energy to $OsH_2 + H_2$ is as high as that to the atomic Os and two H_2 molecules.

The ground state of the D_{4h} structure is $^5B_{1g}$ and the main electron configuration is

$$(\text{core})(\text{Os5s})^2(\text{Os5p})^6(a_{1g})^2(b_{1g})^2(e_u)^4(e_g)^2(a_{1g})^1(b_{2g})^1.$$

From this configuration, eight electronic states ($^1A_{1g}$, $^1A_{2g}$, $^3B_{1g}$, $^1B_{2g}$, $^3A_{1g}$, $^3A_{2g}$, $^5B_{1g}$, and $^3B_{2g}$) arise and the calculated result is consistent with Hund's rule, even after the effects of dynamic correlation are considered at the MRMP2 level of theory. The spin multiplicity of this ground state is interestingly high and intersystem crossings apparently need to occur from the quintet state into a triplet and sequentially into a singlet in order to reach the ground state $^1A_1$ at the most stable T_d structure.

The MCSCF/SBKJC force constant matrix for the ground state at the D_{4h} structure provides three imaginary-frequency modes: a_{2u} (675i cm^{-1}), b_{2u} (704i cm^{-1}), and e_u (779i cm^{-1}),

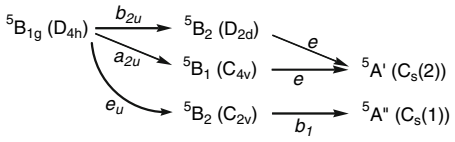

Scheme 2 Geometrical deformation paths from the D_{4h} structure to the T_d structure in OsH_4

where these modes are illustrated in Scheme 1. The geometrical deformations along these modes provide C_{4v}, D_{2d}, and two identical C_{2v} structures, respectively, as discussed in the previous section. The geometrical optimizations of these lower symmetrical structures give the stabilization energies of only 20.1 (C_{4v}), 17.6 (D_{2d}), and 17.3 (C_{2v}) kcal/mol at the MRMP2 level of theory, respectively. Their ground states are assigned as $^5B_1(C_{4v})$,$^5B_2(D_{2d})$, and $^5B_2(C_{2v})$. These geometrical deformations can be explained by the pseudo-Jahn-Teller theory within the adiabatic picture. At the D_{2d} structure, the ground state $^5B_2$ still has one imaginary-frequency mode (e, 405i cm^{-1}) and its structure is deformed into two identical C_s structures (denoted as $C_s(2)$ in Scheme 2 and Fig. 2). The Hessian in the ground state $^5A'$ of this C_s structure is positive definite. At the C_{4v} structure, there is one imaginary-frequency mode (e, 315i cm^{-1}) and its structure is similarly deformed into two identical C_s structures. These are actually $C_s(2)$ illustrated in Fig. 2. The C_{2v} structure also has one imaginary-frequency mode (b_1, 369i cm^{-1}) and its structure is deformed into a different C_s structure (denoted as C_s (1) in Scheme 2 and Fig. 2). The Hessians of these C_s structures are positive definite. Thus, there is no path to reach a T_d structure on the potential energy surface of the lowest quintet state.

In order to reach the ground state of the T_d structure, the lowest singlet potential energy surface needs to be considered; the lowest singlet state ($^1A_{1u}$) at the D_{4h} structure is higher in energy than the ground state by more than 60 kcal/mol. This state belongs to B_1 at the D_{2d} structure and never reaches the ground state $^1A_1$ at the T_d structure. Since the heavy element Os is included, a fast intersystem crossing is expected to occur in this molecule. Therefore, the relativistic potential energy curves were calculated along the deformation path from the D_{4h} to the T_d structure with the Z_{eff} approximation for SOC effects in the present investigation. The deformation path is defined as two H–Os–H angles and the Os–H bond lengths are simultaneously and linearly changed from the D_{4h} to the T_d structure, where this path is often called a linear synchronous transit. Along this path, the two H–Os–H angles perpendicular to each other are 180° at the D_{4h} and 109.5° at the T_d structure, and the molecular symmetry is kept as D_{2d} along this deformation path.

The MCSCF orbitals were optimized with state-averaged technique for the lowest $^1A_{1g}(^1A_1)$,$^3E_g(^3E)$, and $^5B_{1g}(^5B_2)$ states at the $D_{4h}(D_{2d})$ structure, along the deformation path.

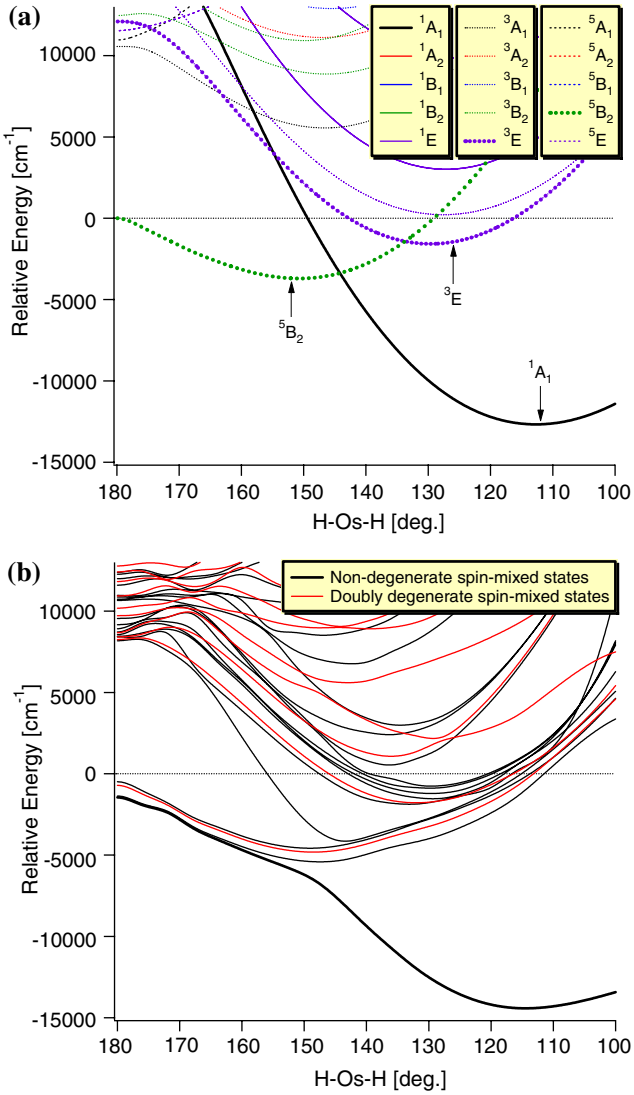

Fig. 3 Potential energy curves along the D_{2d} deformation path from the D_{4h} structure to the T_d structure in OsH_4 obtained using the MCSCF/SBKJC method: **a** adiabatic curves and **b** relativistic curves. The definition of the path is described in the text

As depicted in Fig. 3a, the energy minimum on the lowest adiabatic quintet state $^5B_2$ appears at the H–Os–H angle of about 150°. At this geometry, the $^5B_2$ state is still the ground state in the molecular system, but the potential energy curves of the lowest $^1A_1$ and ^3E states are rapidly lowered along the deformation path as shown in Fig. 3a. The potential energy curves of these three states run across each other at the H–Os–H angle of about 145°. When the SOCs are considered, the potential energy curve of the lowest spin-mixed state monotonically decreases along this path, as shown in Fig. 3b. The avoided crossing between the spin-mixed states whose main components are the lowest $^5B_2$ and $^1A_1$ states, can be explained as follows: the spin-lowering operator in the

Breit-Pauli Hamiltonian provides the interactions between quintets and triplets:

$$\ell_+ s_- = (\ell_x + i\ell_y)s_- = \ell_x s_- + i\ell_y s_-$$

$$= \left(y\frac{\partial}{\partial z} - z\frac{\partial}{\partial y}\right)s_- + i\left(z\frac{\partial}{\partial x} - x\frac{\partial}{\partial z}\right)s_-$$

Since $(x, y) \in E$ and $z \in B_2$ in the D_{2d} symmetry, the one-electron spin-orbit integrals are non-zero between the $^5B_2$ and ^3E states: the present calculations provide

$$\left|\left\langle {}^3\mathrm{E}(m_s = 1)|\mathrm{H_{SO}}|{}^5\mathrm{B}_2(m_s = 2)\right\rangle\right| = 1,206\,\mathrm{cm}^{-1},$$

$$\left|\left\langle {}^3\mathrm{E}(m_s = 0)|\mathrm{H_{SO}}|{}^5\mathrm{B}_2(m_s = 1)\right\rangle\right| = 853\,\mathrm{cm}^{-1}, \text{ and}$$

$$\left|\left\langle {}^3\mathrm{E}(m_s = 1)|\mathrm{H_{SO}}|{}^5\mathrm{B}_2(m_s = 0)\right\rangle\right| = 492\,\mathrm{cm}^{-1},$$

where the same values were obtained for negative m_s values. Furthermore, one-electron spin-orbit integrals are also non-zero between the ^3E and $^1A_1$ states: the present calculations provide

$$\left|\left\langle {}^1\mathrm{A}_1(m_s = 0)|\mathrm{H_{SO}}|{}^3E(m_s = 1)\right\rangle\right| = 2,122\mathrm{cm}^{-1},$$

where the same values were obtained for negative m_s values. As shown in Fig. 3a, the potential energy curve of the ^3E state comes closer in energy to those of both the $^1A_1$ and $^5B_2$ states in the area of 130–160°. As a result, the in-direct couplings between the $^5B_2$ and $^1A_1$ states via the ^3E state occur and provide avoided crossings among the low-lying spin-mixed states, as illustrated in Fig. 3b. In fact, the lowest spin-mixed state at H–Os–H=145° has a large contribution of triplets: singlets of 40%, triplets of 38%, and quintets of 22%. Thus, the SOC effects play important roles in driving the geometrical deformation into the most stable singlet state at the T_d structure in OsH_4.

4 Summary

The dissociation energies of MH_4 (M = La, Hf–Hg) were computed using the FORS MCSCF/SBKJC(f,p) and MRMP2 methods at the MCSCF/SBKJC optimized structures. The present calculations showed that of the molecules examined, only four molecules HfH_4, TaH_4, WH_4, and OsH_4 with T_d symmetry are lower in energy than the corresponding dissociation limits. As for ReH_4, however, it seems that more sophisticated study needs to be performed to obtain more definite evidence for the relative energy of interest. In the present investigation, the potential energy surfaces from the D_{4h} to the T_d structure in WH_4 and OsH_4 were explored from both theoretical calculations and symmetry arguments based on the pseudo-Jahn- Teller effect. As for WH_4, it is found that the ground state could be ^3E_g,$^3A_{2g}$, or $^3B_{2g}$ at the D_{4h} structure. The present calculations suggest that the ground state is ^3E_g, and that this state is stabilized by the e_u deformation into a C_{2v} structure ($^3B_1$) and then sequentially to the most stable T_d structure ($^3A_2$). If the molecular system is promoted to the lowest $^3B_{2g}$ state, the D_{4h} structure can directly deform into the most stable T_d structure along the b_{2u} vibrational mode. For OsH_4, the ground-state D_{4h} structure ($^5B_{1g}$) deforms into a D_{2d} structure and the resulting $^5B_2$ state strongly interacts with the lowest ^3E and $^1A_1$ states due to the SOCs. Accordingly, the relativistic potential energy of the ground state (lowest spin-mixed state) results in a decrease monotonically along the D_{2d} deformation path from the D_{4h} to the T_d structure. The theoretical study on HfH_4, TaH_4, and ReH_4 is being achieved and will be reported in the near future.

References

1. Pyykkö P (1988) Chem Rev 88:563
2. Hess BA, Marian CM, Peyerimhoff SD (1995) In: Yarkony DR (ed) Modern electronic structure theory. Part I. World Scientific, Singaore, p 152
3. Marian CM (1977) In: Problem solving in computational molecular science. Wilson S, Diercksen GHF (eds) Kluwer, Dordrecht, p 291
4. Marian CM (2001) In: Reviews in computational chemistry. Vol. 17. Lipowitz KB, Boyd DB Wiley-VCH, New York p 99
5. Fedorov DG, Koseki S, Schmidt MW, Gordon MS (2003) Int Rev in Phys Chem 22: 551–592
6. Fedorov DG, Schmidt MW, Koseki S, Gordon MS (2004) In: Hirao K, Ishikawa Y (eds) Recent advances in relativistic molecular theory, vol 5. World Scientific, Singapore, pp 107–136. ISBN 981-238-709-9
7. Matsunaga N, Koseki S (2004) In: Lipkowitz KB, Larter R, Cundari TR (eds) Reviews in Computational Chemistry. vol 20 Indiana University-Purdue University at Indianapolis (IUPUI), Chap. 2, pp 101–152
8. Quiney HM, Skaane H, Grant IP (1999) Adv Quantum Chem 32:1
9. Autschbach J, Schwarz WHE (2000) Theo Chem 104: 82–88
10. Yanai T, Iikura H, Nakajima T, Ishikawa Y, Hirao K (2001) J Phys Chem 115: 8267–8273
11. Yanai T, Nakajima T, Ishikawa Y, Hirao K (2002) J Chem Phys 116: 10122–10128
12. Abe M, Yanai T, Nakajima T, Hirao K (2004) Chem Phys Lett 388: 68–73
13. Gang C (2004) Phys Lett A 328: 116–122
14. Krekora P, Su Q, Grobe R (2004) Phys Rev A 70:054101
15. Kędziera D (2005) J Chem Phys 123:074109
16. Wolf A, Reiher M (2006) J Chem Phys 124:064102
17. Stevens WJ, Krauss M (1982) Chem Phys Lett 86:320
18. Stevens WJ, Basch H, Krauss M (1984) J Chem Phys 81: 6026–6033
19. Stevens WJ, Basch H, Krauss M, Jasien P (1992) Can J Chem 70: 612–630
20. Cundari TR, Stevens WJ (1993) J Chem Phys 98: 5555–5565
21. Ermler WC, Ross RB, Christiansen PA (1988) Adv Quantum Chem 19:139
22. Ross RB, Powers JM, Atashroo T, Ermler WC, Lajohn LA, Christiansen PA (1990) J Chem Phys 93: 6654–6670
23. Hay PJ, Wadt WR (1985) J Chem Phys 82: 270–283
24. Wadt WR, Hay PJ (1985) J Chem Phys 82: 284–298
25. Hay PJ, Wadt WR (1985) J Chem Phys 82: 299–310
26. Decker SA, Klobukowski M (2001) J Chem Inf Comput Sci 41: 1–7

27. Osanai Y, Noro T, Miyoshi E (2002) J Chem Phys 117: 9623–9629
28. Fedorov DG, Klobukowski M (2002) Chem Phys Lett 360: 223–228
29. Koseki S, Schmidt MW, Gordon MS (1992) J Phys Chem 96: 10768–10772
30. Koseki S, Gordon MS, Schmidt MW, Matsunaga N (1995) J Phys Chem 99: 12764–12772
31. Matsunaga N, Koseki S, Gordon MS (1996) J Chem Phys 104: 7988–7996
32. Koseki S, Schmidt MW, Gordon MS (1998) J Phys Chem A 102: 10430–10435
33. Koseki S, Fedorov DG, Schmidt MW, Gordon MS (2001) J Phys Chem A 105: 8262–8268
34. Koseki S, Ishihara Y, Umeda H, Fedorov DG, Gordon MS (2002) J Phys Chem A 106: 785–794
35. Koseki S, Ishihara Y, Umeda H, Fedorov DG, Schmidt MW, Gordon MS (2004) J Phys Chem A 108: 4707–4719
36. Koseki S, Matsushita T, Gordon MS (2006) J Phys Chem A 110: 2560–2570
37. Koseki S, Matsushita T, Gordon MS (in preparation)
38. Matsushita T, Asada T, Koseki S (2006) J Phys Chem A 110:13295
39. Matsushita T, Asada T, Koseki S (2007) J Phys Chem C 111 (in press)
40. Toyota A, Nakajima T, Koseki S (1984) J Chem Soc Perkin Trans. II. 85–89
41. Koseki S, Kataoka M, Hanamura M, Nakajima T, Toyota A (1984) J Org Chem 49: 2988–2993
42. Kataoka M, Koseki S, Iida K, Nakajima T (1985) Nouv J Chim 9: 135–138
43. Koseki S, Nakajima T, Toyota A (1985) Can J Chem 63: 1572–1579
44. Toyota A, Kataoka M, Koseki S (1992) Chem Lett 791–794
45. Toyota A, Koseki S (1996) J Phys Chem 100: 2100–2106
46. Koseki S, Toyota A (1997) J Phys Chem A 101: 5712–5718
47. Toyota A, Koseki S (1998) J Phys Chem A 102: 490–495
48. Toyota A, Koseki S (1998) J Phys Chem A 102: 6668–6675
49. Toyota A, Koseki S, Shiota M (2000) J Phys Chem A 104: 5343–5350
50. Toyota A, Shiota M, Nagae Y, Koseki S (2001) J Phys Chem A 105: 1334–1342
51. Toyota A, Koseki S, Umeda H, Suzuki M, Fujimoto K (2003) J Phys Chem A 107: 2749–2756
52. Bullock RM, Song JS (1994) J Am Chem Soc 116: 8602–8612
53. Luan L, Song JS, Bullock RM (1995) J Org Chem 60: 7170–7176
54. Cheng TY, Bullock RM (2002) Organometallics 21:2325–2331
55. Esteruelas MA, López AM, Oñate E, Royo E (2005) Inorg Chem 44: 4094–4103
56. Wen TB, Zhou ZY, Lau CP, Jia G (2000) Organometallics. 19:3466–3468
57. Sellmann D, Prakash R, Heinemann FW (2004) J Chem Soc., Dalton Trans. 3991–3996
58. Henriksson KOE, Vörtler K, Dreißigacker S, Nordlund K, Keinonen J (2006) Surf Sci 600:3767–3174
59. Bayse CA, Hall MB (1999) J Am Chem Soc 121: 1348–1358
60. Wang X, Andrews L (2002) J Phys Chem 106: 6720–6729
61. Ruedenberg K, Schmidt MW, Dombek MM, Elbert ST (1982) Chem Phys 71:41, 51, 65
62. Schmidt MW, Gordon MS (1998) Ann Rev Phys Chem 49: 233–266
63. Nakano HJ (1993) Chem Phys 99: 7983–7992
64. Schmidt MW, Baldridge KK, Boatz JA, Elbert ST, Gordon MS, Jensen JH, Koseki S, Matsunaga N, Nguyen KA, Su S, Windus TL, Dupuis M, Montgomery JA Jr., (1993) J Comput Chem 14:1347–1363
65. Andrews L (2004) Chem Soc Rev 33: 123–132
66. Ohanessian G, Brusich MJ, Goddard WA (1990) J Am Chem Soc 112: 7179–7189
67. Wang X, Andrews L (2003) J Phys Chem A 107: 4081–4091
68. Audrews L, Wang X (2003) J Am Chem Soc 125: 11751–11760
69. Gultou-Guichemerre MG, Chambaud G (2005) J Chem Phys 122:204325
70. Li FX, Zhang XG, Armentrout PB (2005) J Phys Chem B 109: 8350–8357
71. Das KD, Balasubramanian K (1990) Chem Phys Lett 172: 372–378
72. Bytheway I, Bacskay GB, Hush NS (1996) J Phys Chem 100: 6023–6031
73. Bayse CA, Hall MB (1998) Organometallics 17: 4861–4868
74. Jacobsen H, Berke H (2002) J Chem Soc Dalton Trans 3117–3122
75. Chertihin GV, Andrews L (1995) J Am Chem Soc 117: 6402–6403
76. Wang XW, Chen CF (1997) Phys Rev B 56: 7049–7052
77. Wang X, Andrews L (2003) J Phys Chem A 107: 4081–4091
78. Heinekey DM, Payne NG, Schulte GK (1988) J Am Chem Soc 110: 2303–2305
79. Visscher L, Dyall KG, Lee TJI (1995) I J Quantum Chem S29: 411–419
80. Diez RP (1998) Chem Phys Lett 287: 542–548
81. Lee YS, McLean AD (1982) J Chem Phys 76:735
82. Ross RB, Ermler WC (1985) J Phys Chem 89: 5202–5206
83. Sadlej AJ (1991) J Chem Phys 95: 2614–2622
84. Casarrubios M, Seijo L (1999) J Chem Phys 110: 784–796
85. Han Y-K, Hirao K (2000) Chem Phys Lett 324: 453–458
86. Witek HA, Nakajima T, Hirao K (2000) J Chem Phys 113: 8015–8025